Final Summary Report
for the project

Flow Tube Studies of Gas Phase Chemical Processes of Atmospheric Importance

supported under
NASA Grant Number:
NAG5-3947

Prepared for

UPPER ATMOSPHERIC RESEARCH PROGRAM
NASA Headquarters
300 E Street, S.W.
Code YS
Washington, DC 20546-0001
Attn: Dr. Michael J. Kurylo, Manager

Principal Investigator:

Mario J. Molina
Massachusetts Institute of Technology
Room 54-1814
77 Massachusetts Avenue
Cambridge, MA 02139
Phone: (617) 253-5081; Fax: (617) 258-6525
Email: <mmolina@mit.edu>

Flow Tube Studies of Gas Phase Chemical Processes of Atmospheric Importance

In this report we summarize the results of the work carried out in our laboratory under the project "Flow Tube Studies of Gas Phase Chemical Processes of Atmospheric Importance."

1. Production of HCl in the OH + ClO reaction

The second and final phase of our studies of the OH + ClO reaction was carried out under this project. In the first phase we measured the branching ratio for production of DCl in the OD + ClO reaction [Lipson *et al.*, 1997]; in the second phase we measured directly the rate constant for the minor channel that produces HCl. The results, summarized below; have been published [Lipson *et al.*, 1997].

The major products of the OH + ClO reaction are HO_2 and Cl (Reaction 1a; $\Delta H°_{298\,K} = -1.3$ kcal mol^{-1}). The minor channel that produces HCl and O_2 is more exothermic (Reaction 1b; $\Delta H°_{298\,K} = -55.8$ kcal mol^{-1}):

$$OH + ClO \rightarrow HO_2 + Cl \qquad (1a)$$

$$OH + ClO \rightarrow HCl + O_2 \qquad (1b)$$

However, Reaction 1b is kinetically unfavorable because two bonds must be broken almost simultaneously; this reaction proceeds most likely through an addition-elimination mechanism via a four-centered transition state. The conversion of ClO to Cl in Reaction 1a is a chain-propagating step in catalytic ozone depletion cycles because ClO and Cl are both active forms of chlorine. In contrast, Reaction 1b converts an active form of chlorine (ClO) into a more stable reservoir species (HCl). Since Reaction 1b is a chain-terminating step, even a relatively small branching ratio would lead to substantially less ozone depletion by chlorine-containing species.

In our earlier investigation of the branching ratio for the OD + ClO reaction [Lipson *et al.*, 1997] we were able to show that Reaction 1b is a kinetically accessible product channel. Because of the atmospheric importance of Reaction 1b and because of the possibility of an isotope effect, we considered it important to carry out branching ratio measurements directly for the OH + ClO reaction. Recent improvements to our experimental technique significantly reduced the HCl background in our system, making it possible to detect the production of very small concentrations of HCl (~10^9 molecule cm^{-3}) from channel 1b. We investigated the branching ratio of Reaction 1 at pressures between 100 and 200 Torr and at a range of temperatures extending to those found in the lower stratosphere, using the turbulent flow - CIMS technique referred to in the introduction. We also carried out statistical rate theory calculations on the OH + ClO reaction system.

Experimental Section. The experimental apparatus is similar to that used in our earlier study [Lipson *et al.*, 1997]; it is shown schematically in Figure 1. However, we made several important modifications to the ClO source that helped to reduce the HCl background in the system by more than an order of magnitude. For example, we removed trace impurities of H_2 in the helium sweep gas used to flush Cl_2 through the microwave discharge, and we switched the movable glass injector to one made out of alumina, reducing the interaction of Cl atoms with the glass walls. Overall, the modifications reduced the HCl background in the system by more than an order of magnitude (from ~5 x 10^{11} to < 4 x 10^{10} molecule cm^{-3}), making it possible to observe production of very small amounts of HCl from Reaction 1b.

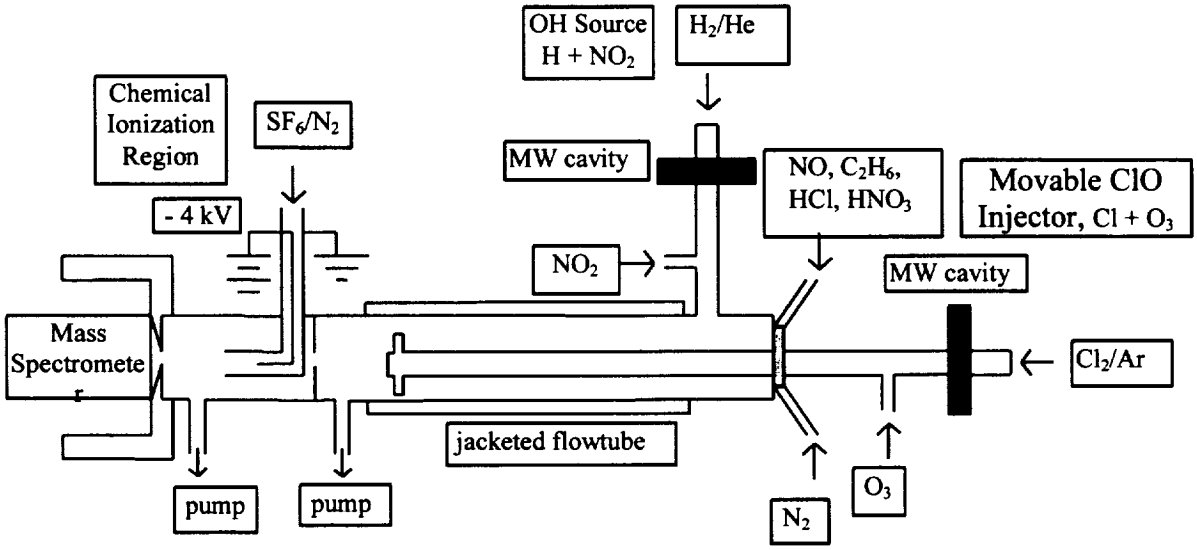

Figure 1. Schematic of experimental apparatus.

The production of HCl background by secondary reactions in the main flow tube was also a concern. The products of the main channel of the OH + ClO reaction are HO_2 and Cl, which can react further to form HCl (k_3 = 3.2 x 10^{-11} cm^3 $molecule^{-1}$ s^{-1}) [DeMore *et al.*, 1997]:

$$HO_2 + Cl \rightarrow HCl + O_2 \qquad (2)$$

On the other hand, the large excess of O_3 (~10^{13} molecule cm^{-3}) used in the production of ClO helped to scavenge Cl atoms produced by Reaction 1a, and therefore, helped to minimize HCl background production from side reactions such as Reaction 2.

Results and Discussion. The observed HCl signal was found to increase linearly over the experimental reaction time, as shown in Figure 2. The branching ratio for the HCl channel was measured under a variety of conditions between 207 and 298 K to ensure that the results were independent of the initial concentrations. In one experiment, close to optimal initial concentrations for OH and ClO were used, such that the observed HCl production was due to Reaction 1b only. In another experiment, the initial OH concentration was increased by 85%, so

that ~20% of the observed HCl production was due to the side reaction HO_2 + Cl. However, both experiments yielded the same rate constant for the minor channel (k_{1b} = 10.2 x 10^{-13} cm^3 $molecule^{-1}$ s^{-1}). Our results yield the Arrhenius expression $k_{1b}(T) = (3.2 \pm 0.8) \times 10^{-13} \exp[(325 \pm 60) / T]$ cm^3 $molecule^{-1}$ s^{-1}. The uncertainty represents the two standard deviation statistical errors in the data and is not an estimate of systematic errors. The negative temperature dependence indicates that the reaction goes through an intermediate complex. The branching ratio has been determined to be 0.07 ± 0.03; it does not appear to have a significant temperature dependence within the error of the measurement.

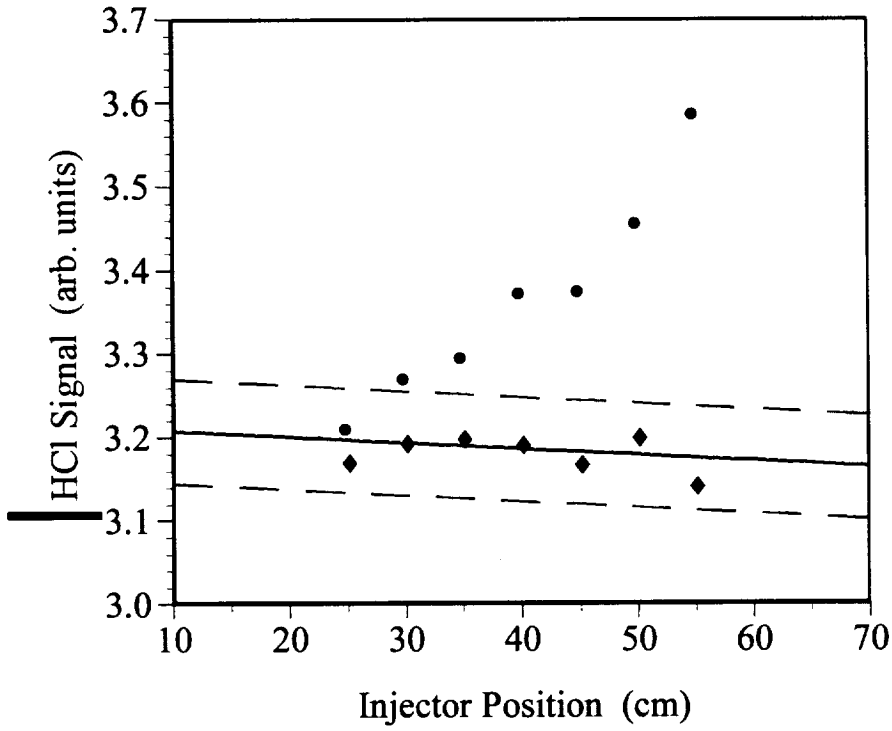

Figure 2. Observed production of HCl ([HCl] = 2.7 x 10^9 molecule cm^{-3}) from Reaction 1b (solid circles) above the small HCl background level (solid diamonds) as a function of injector distance. A least squares fit to the HCl background data was performed, and the dotted lines represent the ± 2σ level. This data set was obtained under the following conditions: P = 97 Torr, T = 298 K, average velocity = 1800 cm s^{-1}, Reynolds number = 3200, $[OH]_o$ = 1.8 x 10^{11} molecule cm^{-3}, $[ClO]_o$ = 8.3 x 10^{11} molecule cm^{-3}.

Modeling by Statistical Rate Theory. The overall reaction is assumed to proceed by way of an addition-elimination mechanism [Dubey et al., 1998]. In order to verify and rationalize the experimentally determined branching ratios and to characterize the influence of isotopic substitution, we performed a detailed modeling, using master equations and statistical rate theory, in collaboration with Professor Matthias Olzmann of Halle-Wittenberg University. Moreover, the temperature and pressure dependence of the overall rate constant was examined,

because an adequate description of these different quantities by a common model could provide additional evidence for the postulated mechanism.

Within this model, Reactions 1a and 1b correspond to the following microscopic steps, where an asterisk denotes vibrational and rotational excitation:

$$OH + ClO \leftrightarrows HOOCl^* \quad (1)$$

$$HOOCl^* \leftrightarrows HO_2 + Cl \quad (1a')$$

$$HOOCl^* \rightarrow HCl + O_2(a^1\Delta_g) \quad (1b')$$

$$HOOCl^* + M \leftrightarrows HOOCl + M \quad (3)$$

Because the electronic ground state of the intermediate, HOOCl, is most likely a singlet state, Reaction 1b' is assumed to yield $O_2(^1\Delta)$ due to spin conservation.

In the following, we describe only briefly the statistical rate theory calculations. The nascent population of HOOCl, f(E), is approximated by a shifted thermal distribution

$$f(E) = \frac{W_{HOOCl}(E - E_{0(-1)}) \exp\left[\frac{-(E - E_{0(-1)})}{k_B T}\right]}{\int_0^\infty W_{HOOCl}(\varepsilon) \exp\left(\frac{-\varepsilon}{k_B T}\right) d\varepsilon}$$

where $E_{0(-1)}$ represents the threshold energy for Reaction -1 and W_{HOOCl} denotes the sum of states of HOOCl; k_B is Boltzmann's constant. The specific unimolecular rate constants are calculated by statistical rate theory as

$$k_r(E) = \frac{W_r(E - E_{0(r)})}{h\, \rho_{HOOCl}(E)}$$

with the density of states of the intermediate ρ_{HOOCl} and Planck's constant h. For the number of open reaction channels W_r, one has to distinguish between two different cases. Reactions -1 and 1a' are simple bond fissions and W_r is calculated by the statistical adiabatic channel model (SACM) in its simplified version. Reaction 1b', on the other hand, proceeds through a well-defined transition-state configuration, and accordingly, $W_{1b'}$ is identified with its sum of states (RRKM model).

The calculations show that the temperature dependence of the branching ratio is very weak, which is in agreement with the experimental findings. This can be explained by inspecting the specific rate constants for the two product channels as a function of energy: a shift of the reactant population to higher energies by increasing the temperature will hardly change the branching ratio. The calculations also show that the isotope effect is very weak. The calculated yields for

OD + ClO are, on an absolute scale, only ~1% lower than those for OH + ClO. This is again in agreement with the experimental findings.

By averaging the specific rate constants over the molecular distributions, a lifetime of ~ 5 ps can be estimated for the vibrationally excited HOOCl* generated from ClO + OH. Therefore, collisional stabilization is negligible under atmospheric conditions, and the branching ratios are virtually independent of pressure. The results also reveal that the overall rate constant for OH + ClO under atmospheric conditions is not in its high-pressure limit, since ~30 to ~45% redissociation occurs, depending on the temperature.

Conclusions. Our results indicate that the minor channel for the OH + ClO reaction is indeed significant. The branching ratio involving the production of HCl was determined to be 7% under stratospheric conditions. Statistical rate theory calculations have shown that theoretical predictions are in good agreement with the experimental results. Numerous atmospheric modeling studies have proposed that a branching ratio close to 7% would resolve discrepancies between measured and calculated chlorine partitioning in the upper stratosphere and help to resolve some of the discrepancies between measured and calculated O_3 concentrations, especially near 40 km. This work should help to improve modeling of O_3 levels in the upper stratosphere by placing more stringent constraints on the partitioning of stratospheric chlorine.

2. Quantum yields in the photolysis of Cl_2O

Although the chemistry of Cl_2O (dichlorine monoxide) is not of direct relevance to the stratosphere, a study of its photodissociation should further the understanding of the photochemistry of similar molecules. Nickolaisen *et al.* [1996a] reported recently that broadband photolysis of this species at wavelengths beyond 300 nm results in a quantum yield that decreases with pressure. Furthermore, they reported a transient absorption spectrum that they assigned to a metastable triplet state of Cl_2O. If this is the case, these results would imply that the quantum yield for photodecomposition is less than unity at atmospherically relevant wavelengths, in contrast with the normal expectation resulting from the continuous nature of the absorption spectrum at those wavelengths. In fact, Nickolaisen *et al.* [1996b] also reported a similar situation for $ClONO_2$; if it turns out that the photodecomposition quantum yield for this species is less than unity, the atmospheric implications would be quite important.

In order to further resolve the nature of the photolysis of Cl_2O in the 300 nm wavelength region of the spectrum, we employed a broadband light source with a monochromator for wavelength discrimination. Detection and measurement of the yields of the photofragments were accomplished by flowing the reactant Cl_2O in a N_2 carrier gas through a photolysis tube attached to the monochromator, and by monitoring the products with CIMS. Photolysis of Cl_2O yields a chlorine atom and a ClO radical:

$$Cl_2O + h\nu \rightarrow Cl + ClO \qquad (4)$$

Measurements of the yields of both photolysis products were carried out with two different titration schemes. In the first one excess ethane ($[C_2H_6] \sim 300x[Cl_2O]$) was added to the Cl_2O/N_2 flow in order to convert nearly all of the Cl to HCl:

$$Cl + C_2H_6 \rightarrow HCl + C_2H_5\bullet \qquad (5)$$

It was then possible to detect both photolysis products using SF_6^- as the reactant ion, with ClO appearing as ClO^- and Cl (titrated to HCl) as SF_5Cl^-:

$$SF_6^- + ClO \rightarrow ClO^- + SF_6 \qquad (6)$$

$$SF_6^- + HCl \rightarrow SF_5Cl^- + HF \qquad (7)$$

In the second titration scheme no ethane was added, and the Cl formed from photolysis reacted with the Cl_2O:

$$Cl + Cl_2O \rightarrow Cl_2 + ClO \qquad (8)$$

The ClO was effectively amplified by a factor of two (assuming complete reaction of all Cl), and the Cl was converted to the stable molecule Cl_2. The ClO was detected as ClO^- (through Reaction 6) and the Cl_2 was detected as Cl_2^-:

$$SF_6^- + Cl_2 \rightarrow Cl_2^- + SF_6 \qquad (9)$$

With each of these two titration schemes it was possible to measure *both* photolysis product yields under the same conditions. This capability offered a consistency check between the two schemes as well as within each scheme.

Experimental. Cl_2O was synthesized by condensing Cl_2 onto freshly prepared, dried, yellow mercuric oxide and allowing them to react overnight at 196 K [Schack and Lindahl, 1967]. Unreacted Cl_2 was removed from Cl_2O by successive vacuum distillations. The purity of the Cl_2O sample was determined to be at least 99% with UV absorption spectroscopy and CIMS.

A 75-W xenon arc lamp (Oriel 6137) produced white light that was focused into a monochromator (McKee-Pedersen Instruments 1018B) fitted with a 2360 lines/mm diffraction grating. The photolysis tube positioned at the exit slit of the monochromator was constructed from 0.25-inch o. d. Pyrex tubing with quartz windows at each end. The light flux was measured at the end of the tube with a calibrated photodiode (Oriel 70282). The concentration of Cl_2O in the photolysis tube was typically $3\text{-}10 \times 10^{15}$ molecule cm^{-3}. The entire flow passed down the length of the tube and then entered the ion-molecule region; the CIMS apparatus was similar to that described in our previous studies [Seeley *et al.*, 1996; Elrod *et al.*, 1996; Percival *et al.*,

1997]. Under typical operating conditions, the pressure in the photolysis tube and in the ion-molecule region was ~ 50 Torr.

Results and Discussion. Relative quantum yield calculations were carried out for each of the products through comparison with product yields measured at the reference wavelength (255 nm). This reference wavelength was chosen for the following reasons: (1) Cl_2O possesses an absorption maximum very near to this wavelength, and (2) the effect of pressure on the photodissociation of Cl_2O reported by Nickolaisen et al. is negligible at 255 nm. The wavelength of the radiation in the photolysis tube was alternated between the reference and measurement wavelengths; since only the wavelength was changed, this procedure allowed other variables (including gas flows and concentrations) to be kept relatively constant between successive measurements.

In order to minimize the effect of differences in the secondary chemistry, the ClO concentration (as measured by the ClO^- signal) was matched at the two wavelengths by attenuation of the light at the reference wavelength with a neutral density filter of variable optical density. With comparable concentrations of all trace species at the two wavelengths, similar detection sensitivities and secondary chemistry was ensured. This procedure allowed a direct comparison of photolysis-titration product yields at the two wavelengths. Sample measurements are shown in Figure 3.

Table 1 lists the quantum yields determined at the four measurement wavelengths relative to that at the reference wavelength of 255 nm, for both products and for each of the two titration schemes. The uncertainties shown represent 95% confidence limits and include estimated uncertainties in the measurement of the light flux as well as estimated uncertainties in the Cl_2O absorption cross sections, as published in the literature [Lin, 1976]. As only the ratio of the cross sections is needed for the calculations, the uncertainty in the absolute value of the cross section represents a conservative estimate. It turns out that the uncertainties in the published cross section data contribute a significant amount to the overall uncertainty in the determination of the relative quantum yields.

Our measurements indicate that the quantum yield for production of both Cl and ClO from the photodissociation of Cl_2O is essentially constant at all wavelengths. The yields at the various measurement wavelengths agree well with the yield at the reference wavelength, as well as with each other. In addition, the yields calculated from the measurements of the Cl and ClO fragments are consistent with one another, indicating that there is no unaccounted for secondary chemistry present.

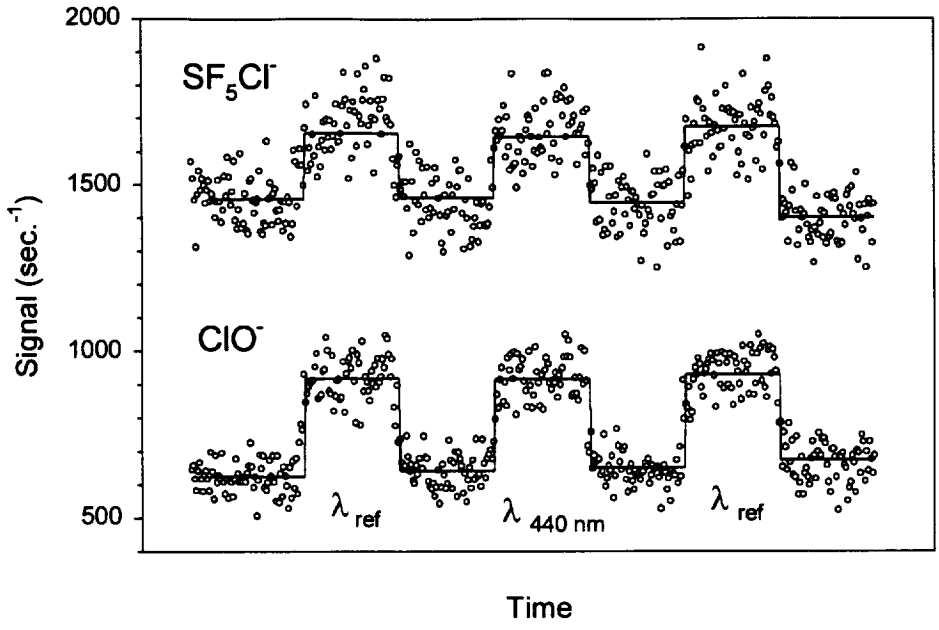

Figure 3. Sample signal rise for the detection of ClO as ClO^-, and Cl as SF_5Cl^-, at the reference (255 nm) and measurement (440 nm) wavelengths. The solid line represents the average signal with the photolysis radiation on and off.

Table 1. Measured Cl_2O quantum yields (relative to that at 255 nm) at 50 Torr total pressure

λ	With C_2H_6		Without C_2H_6	
	$\Phi(ClO^-)$	$\Phi(SF_5Cl^-)$	$\Phi(ClO^-)$	$\Phi(Cl_2^-)$
320	0.98 ± 0.10	1.08 ± 0.16	0.95 ± 0.13	0.95 ± 0.18
360	1.04 ± 0.14	1.02 ± 0.19	1.06 ± 0.18	0.99 ± 0.15
400	1.02 ± 0.14	0.94 ± 0.16	1.06 ± 0.19	1.12 ± 0.16
440	1.06 ± 0.14	0.97 ± 0.13	1.17 ± 0.17	1.04 ± 0.17

In the broadband flash photolysis experiments conducted by Nickolaisen *et al.*, [ClO]/Cl_2O] yields were observed to decrease with increasing pressure. In fact, the yields reported decreased by more than an order of magnitude from 5 Torr to 100 Torr in some of their measurements. The decrease appeared to be more pronounced at longer wavelengths, and it was proposed that these variations are evidence of a metastable excited state of Cl_2O. This metastable state would experience competition between dissociation and quenching processes:

$$Cl_2O + h\nu \rightarrow Cl_2O^{\dagger} \qquad (10)$$

$$Cl_2O^{\dagger} \rightarrow Cl + ClO \qquad (11)$$

$$Cl_2O^{\dagger} + M \rightarrow Cl_2O + M \qquad (12)$$

Nickolaisen *et al.* argued that the dissociation of the excited Cl_2O is effectively less efficient at longer wavelengths, so that the pressure dependent quenching is enhanced and ClO yields are reduced. In contrast, the results of our experiments indicate that there is no change in the quantum yield from 255 nm to 440 nm at a pressure of 50 Torr (where quenching should be significant). At the moment we do not have a satisfactory explanation for the discrepancy.

This material has been submitted for publication in the Journal of Physical Chemistry.

3. Quantum yield for production of $O(^1D)$ in the photolysis of ozone

Solar radiation that penetrates to the lower atmosphere ($\lambda > 290$ nm) can dissociate O_3 through the following four photolysis pathways:

$$O_3 + h\nu \rightarrow O(^1D) + O_2(^1\Delta_g) \qquad \lambda \leq 310 \text{ nm} \qquad (13)$$

$$\rightarrow O(^1D) + O_2(^3\Sigma_g^-) \qquad \lambda \leq 411 \text{ nm} \qquad (14)$$

$$\rightarrow O(^3P) + O_2(^1\Delta_g) \qquad \lambda \leq 611 \text{ nm} \qquad (15)$$

$$\rightarrow O(^3P) + O_2(^3\Sigma_g^-) \qquad \lambda \leq 1180 \text{ nm} \qquad (16)$$

The production of excited oxygen atoms, $O(^1D)$, leads to the formation of OH radicals through reaction with water vapor:

$$O(^1D) + H_2O \rightarrow OH + OH \qquad (17)$$

At wavelengths greater than 290 nm the solar actinic flux increases rapidly while both the O_3 absorption cross section and the $O(^1D)$ quantum yield decrease substantially. Therefore, $O(^1D)$ production can be influenced considerably by the value of the quantum yield in this region of the spectrum.

The photolysis of ozone has been studied for decades with main focus on the measurement of $O(^1D)$ yields [see, e.g., Ravishankara *et al.*, 1998; DeMore *et al.*, 1997]. Photolysis occurs predominantly through Reaction 13 at $\lambda < 310$ nm, the thermodynamic threshold for this channel. However, $O(^1D)$ quantum yields greater than zero have been measured at wavelengths as long as 330 nm. Recent work has concentrated on quantitatively determining the yield in this "tail" region and in identifying the contributions of Reaction 13 (spin-allowed) and Reaction 14 (spin-forbidden) to $O(^1D)$ yields [Armerding *et al.*, 1995; Silvente *et al.*, 1997; Ball *et al.*, 1997; Denzer *et al.*, 1998]. Most recently, Takahashi *et al.* [1998] used laser induced fluorescence to detect the $O(^3P)$ and $O(^1D)$ photofragments directly at 305-329 nm and at various temperatures; they were able to assign $O(^1D)$ yields from both Reactions 13 and 14. Talukdar *et al.* [1997] also

measured $O(^1D)$ yields at similar wavelengths and temperatures using resonance fluorescence to detect $O(^1D)$ quenched to $O(^3P)$ and laser induced fluorescence to detect $O(^1D)$ as OH.

In an effort to further characterize the production of $O(^1D)$ in this tail region of the spectrum, we have employed a broadband light source with a monochromator for wavelength discrimination, using essentially the same experimental technique as described above for the Cl_2O quantum yield measurements. We describe here our room-temperature results; we are in the process of extending the measurements to lower temperatures.

We titrated selectively the $O(^1D)$ with excess N_2O to produce NO_2 and NO_3:

$$O(^1D) + N_2O \rightarrow NO + NO \quad (18)$$

$$\rightarrow N_2 + O_2 \quad (19)$$

$$NO + O_3 \rightarrow NO_2 + O_2 \quad (20)$$

$$NO_2 + O_3 \rightarrow NO_3 + O_2 \quad (21)$$

Subsequent detection and measurement of the titration products was accomplished with CIMS. In the ion-molecule region O_3^- ionized NO_2 and NO_3 to form NO_3^-, which was subsequently monitored with the mass spectrometer:

$$O_3^- + NO_2 \rightarrow NO_3^- + O_2 \quad (22)$$

$$O_3^- + NO_3 \rightarrow NO_3^- + O_3 \quad (23)$$

Thus, the $O(^1D)$ photofragment was selectively transformed into NO_3^- through a series of titration reactions.

Experimental. The apparatus is the same as that described briefly in the Cl_2O section. The O_3 was introduced by passing a carrier flow of Ar (UHP Matheson) through the trap where it was stored. The O_3/Ar flow (10 sccm) and N_2O (UHP Matheson) flow (5 sccm) were introduced and mixed at the rear of the photolysis tube. The concentration of O_3 in the photolysis tube was typically 1-5 x 10^{16} molecule cm^{-3}. The primary reagent ion SF_6^- reacted to near completion in the presence of excess O_3 to produce the main reagent ion, O_3^-:

$$SF_6^- + O_3 \rightarrow O_3^- + SF_6 \quad (24)$$

Results and Discussion. Relative quantum yield measurements were made by comparison of the NO_3^- yields at various wavelengths relative to the yield at a reference wavelength, 300 nm. This reference wavelength was chosen for several reasons: first, the O_3 absorption cross section is fairly large at this wavelength (4 x 10^{-19} cm^2 at 298 K). Second, the $O(^1D)$ quantum yield is

known to be close to unity (~ 0.9) at this wavelength. Third, the $O(^1D)$ quantum yield is believed to be fairly constant around this wavelength (thus minimizing errors incurred by slight wavelength shifts). All measurements were placed on an absolute scale by normalizing at 308 nm, where previous studies have fixed the quantum yield at 0.79 [DeMore et al., 1997].

As was the case with our Cl_2O measurements, the wavelength of the light in the photolysis tube was alternated between the reference and measurement wavelengths, and the NO_3^- signal was matched at the two wavelengths by attenuation of the light at the reference wavelength with a neutral density filter. All measurements were conducted at a pressure of 50 Torr and a temperature of 298 K (±3 K); the measured quantum yields were normalized to a value of 0.79 at 308 nm. The wavelength resolution varied from ± 0.05 nm to ± 1.6 nm, and the quantum yields reported actually represent an average value over the corresponding wavelength range. Figure 5 shows these quantum yields at the wavelengths studied here along with data from other studies for comparison. Figure 6 shows the behavior of the quantum yield in the tail region (315 nm $\leq \lambda \leq$ 330 nm). The uncertainties represent 95% confidence limits and include estimated uncertainties in the measurement of the light flux, as well as in the O_3 absorption cross sections as reported in the literature [Molina and Molina, 1986; Caccianni *et al.*, 1989].

The $O(^1D)$ quantum yield measurements described here support recent work indicating a value greater than zero in the 310 - 330 nm wavelength range. Furthermore, our measurements corroborate this finding at wavelengths up to 351 nm. In this region there appears to be a nearly constant contribution to the production of $O(^1D)$ of ~ 0.10.

The quantum yields at long wavelengths have been attributed to contributions from vibrational excitation of O_3 and formation of spin-forbidden products (Reaction 14). The recommendation of DeMore *et al.* [1997] is based on a model by Michelsen *et al.* [1994] in which vibrational excitation of the symmetric, asymmetric and bending modes of O_3 is taken into account. The effect of this "hot O_3" contribution on the quantum yield (shown in Figure 5) can be seen with distinct structure appearing near 319, 321 and 323 nm. This structure can be seen in our data and in that of Takahashi *et al.*, and to a lesser degree also in the data of Talukdar *et al.* It therefore seems reasonable to conclude that internal excitation in the O_3 accounts for some of the long-wavelength $O(^1D)$ production.

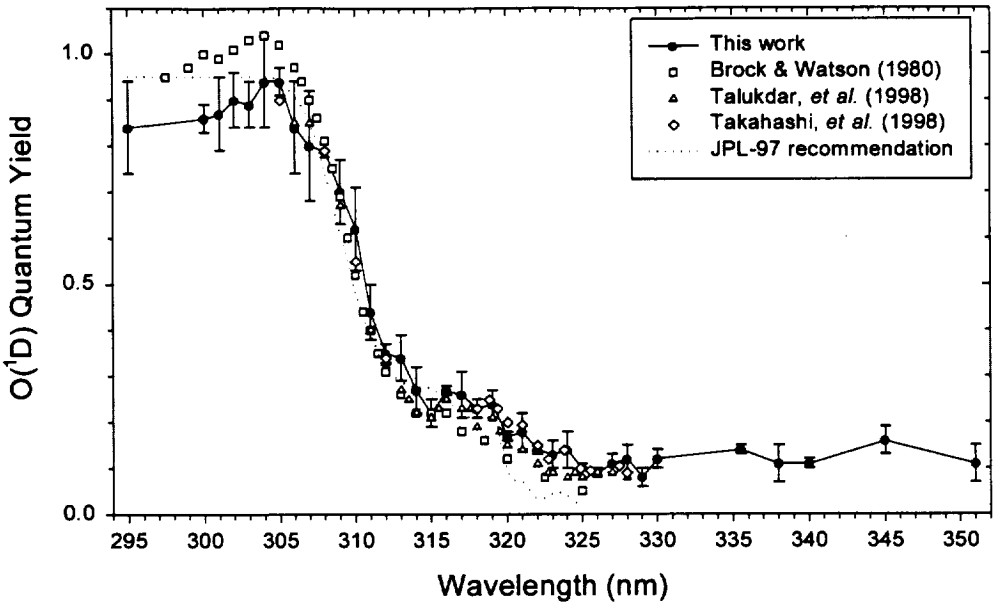

Figure 4. O(^{1}D) quantum yields as a function of wavelength from 295 nm to 351 nm at 298 K.

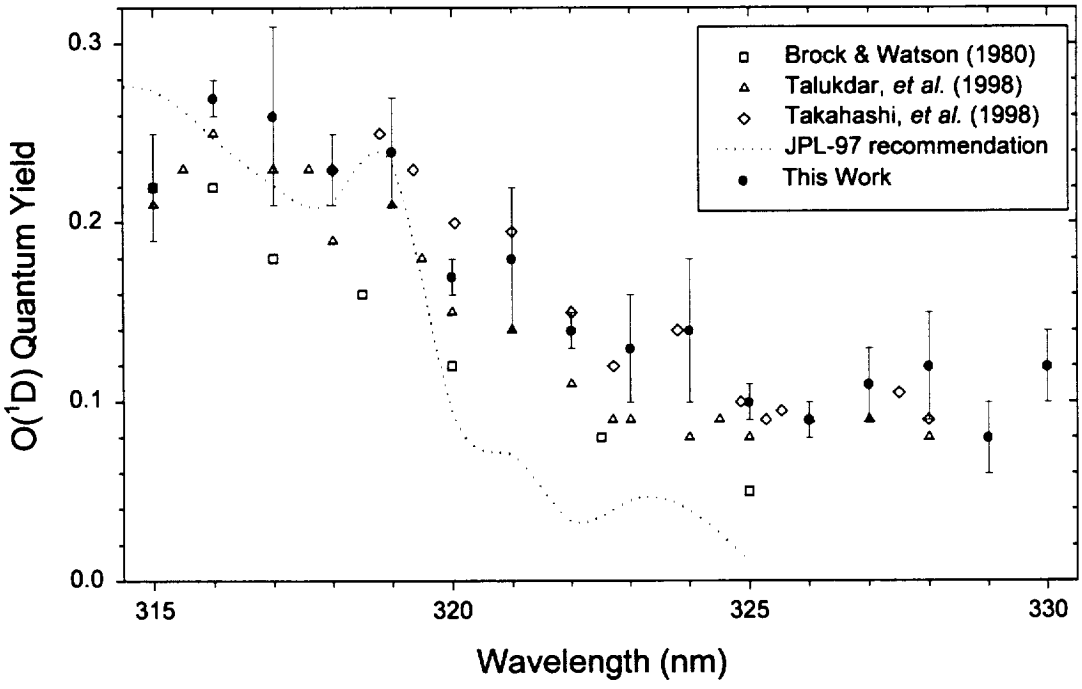

Figure 5. O(^{1}D) quantum yields as a function of wavelength in the tail region at 298 K.

The observation of non-zero values at wavelengths greater than 325 nm and also below room temperature suggests that hot O_3 is not the only source of $O(^1D)$, and that a spin-forbidden process is active. This spin-forbidden contribution (Reaction 14) is expected to be relatively constant at these long wavelengths, since its thermodynamic threshold is at 411 nm. Our measurements indicate a nearly constant $O(^1D)$ quantum yield at wavelengths from 325 nm to 351 nm. These findings are consistent with a spin-forbidden production of $O(^1D)$ at longer wavelengths, though the value of 0.10 is somewhat higher than that suggested by Takahashi *et al.* (0.08) and Talukdar *et al.* (0.06).

Conclusions. Our experimental results on O_3 photolysis in conjunction with the studies of Takahashi et al. [1998] and Talukdar et al. [1997] suggest that two processes contribute to the production of $O(^1D)$ at wavelengths past its thermodynamic threshold. First, structure in the quantum yield at long wavelengths offers evidence that internally excited O_3 can extend dissociation via Reaction 13 (spin allowed) past the 310 nm threshold. Second, a nearly constant quantum yield (~ 0.10) from 325 nm to 351 nm supports the participation at these wavelengths of Reaction 14, the spin-forbidden channel.

This material has been submitted for publication to the Journal of Physical Chemistry.

4. The CH_3O_2 + NO reaction

The atmospheric oxidation of most hydrocarbons in the presence of nitrogen oxides involves (1) abstraction of a hydrogen atom by OH radicals; (2) addition of O_2 to form a peroxy radical; (3) reaction of the peroxy radical with NO to form NO_2; and (4) photolysis of NO_2 to form O-atoms, and subsequently, ozone. In the case of methane, the reactions are as follows:

$$CH_4 + OH \rightarrow CH_3 + H_2O \qquad (25)$$

$$CH_3 + O_2 + M \rightarrow CH_3O_2 + M \qquad (26)$$

$$CH_3O_2 + NO \rightarrow CH_3O + NO_2 \qquad (27)$$

$$NO_2 + h\nu \rightarrow NO + O \qquad (28)$$

$$O + O_2 + M \rightarrow O_3 + M \qquad (29)$$

The rate constant for Reaction 27 has been measured by several groups [see DeMore *et al.*, 1997]; the agreement is reasonable. Villalta *et al.* [1995] and Scholtens *et al.* [1999] employed a flowtube-CIMS technique to determine the rate constant, obtaining (7.5 ± 1.3) and (7.8 ± 2.2) x 10^{-12} cm^3 $molecule^{-1}$ s^{-1} respectively. The focus of the latter study was to investigate the branching channel for Reaction 27 to form CH_3ONO_2; the authors were able to establish an upper limit of 0.03 for the branching ratio.

We have measured the rate constant for Reaction 27 at room temperature (298 K) using our turbulent flow-CIMS approach in order to gain familiarity with chemical ionization scheme for hydrocarbon radicals. We employed a UTI 100C mass spectrometer; the flow tube was maintained at ~100 Torr, and the chemical ionization region at ~15 Torr. The parent ion used was O_2^+ and the peroxy radical was detected as CH_3^+, following the ion-molecule scheme reported by Villalta *et al.* [1995]:

$$CH_3O_2 + O_2^+ \rightarrow CH_3O_2^+ + O_2 \quad (25\%) \qquad (30)$$

$$CH_3O_2 + O_2^+ \rightarrow CH_3^+ + 2O_2 \quad (75\%) \qquad (31)$$

The peroxy radicals were generated using a microwave discharge to dissociate molecular fluorine and adding excess methane and oxygen downstream:

$$F_2 \rightarrow 2\,F \qquad (32)$$

$$F + CH_4 \rightarrow CH_3 + HF \qquad (33)$$

$$CH_3 + O_2 + M \rightarrow CH_3O_2 + M \qquad (26)$$

Typical experimental conditions were $[F_2] = 3 \times 10^{11}$ molecule cm^{-3}; $[CH_4] = 6 \times 10^{11}$ molecule cm^{-3}; $[O_2] = 6 \times 10^{16}$ molecule cm^{-3}; $[NO] = 7\text{-}70 \times 10^{11}$ molecule cm^{-3}. The NO reactant was introduced through a moveable injector, and the subsequent CH_3O_2 decays were monitored with the mass spectrometer; the results are shown in Figure 6. To insure pseudo-first order decays the NO concentration was a factor of 10 larger than the CH_3O_2 concentration. The second order rate coefficient inferred from the decay data is $k = 6.0 \times 10^{-12}$ cm^3 $molecule^{-1}$ s^{-1}, with an estimated uncertainty of 30%. Inspection of the figure shows, however, that the decays are not exponential. The slight curvature in the log-plots is most likely a consequence of signal interference in the CH_3^+ mass channel. The CH_3O_2 reaction sequence proceeds as follows:

$$CH_3O_2 + NO \rightarrow CH_3O + NO_2 \qquad (34)$$

$$CH_3O + NO + M \rightarrow CH_3ONO + M \qquad (35)$$

$$CH_3O + O_2 \rightarrow CH_2O + HO_2 \qquad (36)$$

$$CH_3O + NO_2 + M \rightarrow CH_3ONO_2 + M \qquad (37)$$

The reaction products CH_3ONO and CH_3ONO_2 probably react with the O_2^+ to form CH_3^+ as well, thus explaining the non-exponential CH_3O_2 decays at high NO concentrations. Confining the data to low NO concentrations yields $k \sim 7 \times 10^{-12}$ cm^3 $molecule^{-1}$ s^{-1}, in very good agreement with the value reported in earlier studies.

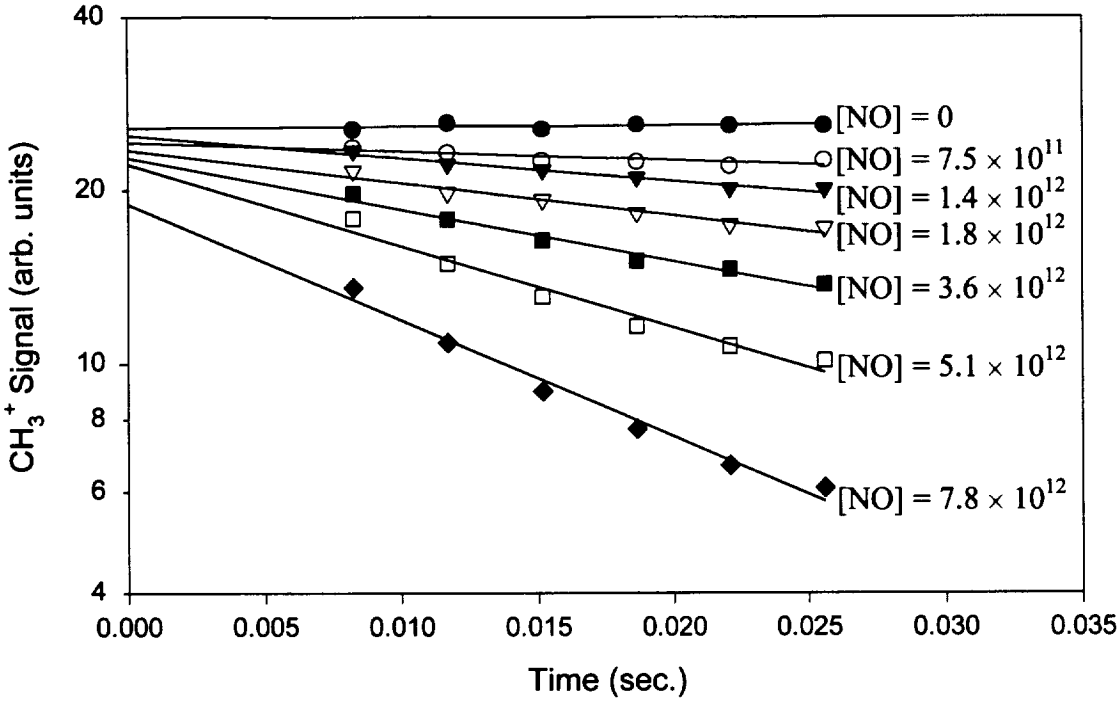

Figure 6. CH_3O_2 decays, measured as CH_3^+ signal, for various NO concentrations.

In summary, we have shown that methyl peroxy radicals can be measured with high sensitivity with our CIMS apparatus. On the other hand, it is clear that the data have to be interpreted very carefully when the product ion mass is not the same as that of the neutral species under investigation, because of the possibility of multiple species contributing to the ion signal.

5. Kinetics of the ClO + NO_2 and ClO + HO_2 reactions

We have measured the temperature and pressure dependence of the rate constant for the ClO + NO_2 reaction using the turbulent flow-CIMS technique. The results have been published [Percival *et al.*, 1997] and are in excellent agreement with the values recommended by the NASA Panel for Data Evaluation [DeMore *et al.*, 1997].

We are currently measuring the rate constant for the ClO + HO_2 reaction using essentially the same flowtube-CIMS approach.

6. REFERENCES

Armerding, W., F.J. Comes, and B. Schülke, $O(^1D)$ quantum yields of ozone photolysis in the UV from 300 nm to its threshold and at 355 nm, *J. Phys. Chem.*, **99**, 3137-3143, 1995.

Ball, S.M., G. Hancock, S.E. Martin, and J.C. Pinot de Moira, A direct measurement of the $O(^1D)$ quantum yields from the photodissociation of ozone between 300 and 328 nm, *Chem. Phys. Lett.*, **264**, 531, 1997.

Caccianni, M., A. Di Sarra, A., G. Fiocco, A. Amoruso, Absolute Determination of the Cross Sections of Ozone in the Wavelength Region 339-355 nm at Temperatures 220-293 K, *J. Geo. Res.*, **94**, 8485-8490, 1989.

DeMore, W.B., D.M. Golden, R.F. Hampson, C.J. Howard, C.E. Kolb, M.J. Kurylo, M.J. Molina, A.R. Ravishankara, and S.P. Sander, Chemical kinetics and photochemical data for use in stratospheric modeling, *JPL Publ. 97-4, Evaluation Number 12*, 1997.

Denzer, W., G. Hancock, J.C. Pinot de Moira, and P.L. Tyley, Spin-forbidden dissociation of ozone in the Huggins bands, *Chem. Phys.*, **231**, 109-119, 1998.

Dubey, M.K., M.P. McGrath, G.P. Smith, and F.S. Rowland, HCl yield from OH + ClO: Stratospheric model sensitivities and elementary rate theory calculations, *J. Phys. Chem.*, **102**, 3127, 1998.

Elrod, M.J., R.F. Meads, J.B. Lipson, J.V. Seeley, and M.J. Molina, Temperature dependence of the rate constant for the HO_2 + BrO reaction, *J. Phys. Chem.*, **100**, 5808-5812, 1996.

Lin, C., Extinction Coefficients of Chlorine Monoxide and Chlorine Heptoxide, *J. Chem. Eng. Data*, **21**, 411-413, 1976.

Lipson, J.B., M.J. Elrod, T.W. Beiderhase, L.T. Molina, and M.J. Molina, Temperature dependence of the rate constant and branching ratio for the OH + ClO reaction, *J. Chem. Soc., Faraday Trans.*, **93**, 2665-2673, 1997.

Lipson, J.B., T.W. Beiderhase, L.T. Molina, M.J. Molina, and M. Olzmann, Production of HCl in the OH + ClO reaction: Laboratory measurements and statistical rate theory calculations, *J. Phys. Chem.*, **103**, 6540-6551, 1999.

Michelsen, H.A., R.J. Salawitch, P.O. Wennberg, and J.G. Anderson, Production of $O(^1D)$ from Photolysis of O_3, *Geophys. Res. Lett.*, **21**, 2227-2230, 1994.

Molina, L.T., and M.J. Molina, Absolute absorption cross sections of ozone in the 185- to 350-nm wavelength range, *J. Geophys. Res.*, **91**, 14501-14508, 1986.

Nickolaisen, S.L., C.E. Miller, S.P. Sander, M.R. Hand, I.H. Williams, and J.S. Francisco, Pressure dependence and metastable state formation in the photolysis of dichlorine monoxide (Cl_2O), *J. Chem. Phys.*, **104**, 2857-2868, 1996a.

Nickolaisen, S.L., S.P. Sander, and R.R. Friedl, Pressure-dependent yields and product branching ratios in the broadband photolysis of chlorine nitrate, *J. Phys. Chem.*, **199**, 10,165-10,178, 1996b.

Percival, C.J., G.D. Smith, L.T. Molina, and M.J. Molina, Temperature and pressure dependence of the rate constant for the ClO and NO_2 reaction, *J. Phys. Chem.*, **101**, 8830, 1997.

Ravishankara, A.R., G. Hancock, M. Kawasaki, and Y. Matsumi, Photochemistry of ozone: Surprises and recent lessons, *Science*, **280**, 60-61, 1998.

Schack, C.J., and C.B. Lindall, On the synthesis of chlorine monoxide, *Inorg. Nucl. Chem. Lett.*, **3**, 387-389, 1967.

Scholtens, K.W., B.M. Messer, C.D. Cappa, and M.J. Elrod, Kinetics of the CH_3O_2 + NO reaction: Temperature dependence of the overall rate constant and an improved upper limit for the CH_3ONO_2 branching channel, *J. Phys. Chem. A*, **103**, 4378, 1999

Seeley, J.V., R.F. Meads, M.J. Elrod, and M.J. Molina, Temperature and pressure dependence of the rate constant for the HO_2+ NO reaction, *J. Phys. Chem.*, **100** (14), 4026-4031, 1996.

Silvente, E., R.C. Richter, M. Zheng, E.S. Saltzman, and A.J. Hynes, Relative quantum yields for $O(^1D)$ production in the photolysis of ozone between 301 and 336 nm: evidence for the participation of a spin-forbidden channel, *Chem. Phys. Lett.*, **264**, 309-315, 1997.

Takahashi, K., N. Taniguchi, Y. Matsumi, M. Kawasaki, and M.N.R. Ashfold, Wavelength and temperature dependence of the absolute $O(^1D)$ production yield from the 305-329 nm photodissociation of ozone, *J. Chem. Phys.*, **108**, 7161-7172, 1998.

Talukdar, R.K., C.A.Longfellow, M.K. Gilles, and A.R. Ravishankara, Quantum yields of $O(^1D)$ in the photolysis of ozone between 289 and 329 nm as a function of temperature, *Geo. Res. Lett.*, **25**, 143-146, 1998.

Villalta, P.W., L.G. Huey, and C.J. Howard, A temperature-dependent kinetics study of the CH_3O_2 + NO reaction using chemical ionization mass spectrometry, *J. Phys. Chem.*, **99**, 12829-12834, 1995.

7. PUBLICATIONS RESULTING FROM THIS AWARD

Lipson, J.B., M.J. Elrod, T.W. Beiderhase, L.T. Molina, and M.J. Molina, Temperature dependence of the rate constant and branching ratio for the OH + ClO reaction, *J. Chem. Soc., Faraday Trans.*, **93**, 2665-2673, 1997.

Lipson, J.B., T.W. Beiderhase, L.T. Molina, M.J. Molina, and M. Olzmann, Production of HCl in the OH + ClO reaction: Laboratory measurements and statistical rate theory calculations, *J. Phys. Chem.*, **103**, 6540-6551, 1999.

Lipson, J.B, Experimental Kinetics Studies of Gas Phase Halogen Reactions, Ph.D. Thesis, MIT, 1999.

Percival, C.J., G.D. Smith, L.T. Molina, and M.J. Molina, Temperature and pressure dependence of the rate constant for the ClO and NO_2 reaction, *J. Phys. Chem.*, **101**, 8830, 1997.

Smith, G.D., Experimental Studies of Photolytic Reactions of Atmospheric Significance using Chemical Ionization Mass Spectrometry. Ph.D. Thesis, MIT, 2000.

Smith, G.D., L.T. Molina and M.J. Molina, Temperature dependence of $O(^1D)$ quantum yields from the photolysis of ozone between 295 and 338 nm, *J. Phys. Chem.*, submitted.

Smith, G.D., L.T. Molina and M.J. Molina, Measurement of Relative Product Yields from the Photolysis of Dichlorine Monoxide (Cl_2O), *J. Phys. Chem.*, submitted.